DOI: 10.1002/chem.200802077

# Probing Hydrogen Bonding to Bound Dioxygen in Synthetic Models for Heme Proteins: The Importance of Precise Geometry

**Henry Dube,[a] Besnik Kasumaj,[b] Carlos Calle,[b] Beatrice Felber,[a] Makoto Saito,[a] Gunnar Jeschke,*[b] and François Diederich*[a]**

*Dedicated to Professor Armin de Meijere at the occasion of his 70th birthday*

**Abstract:** Distal hydrogen bonding in natural dioxygen binding proteins is crucial for the discrimination between different potential ligands such as $O_2$ or CO. In the present study, we probe the chemical requirements for proper distal hydrogen bonding in a series of synthetic model compounds for dioxygen-binding heme proteins. The model compounds **1-Co** to **7-Co** bear different distal residues. The hydrogen bonding in their corresponding dioxygen adducts is directly measured by pulse EPR spectroscopy. The geometrical requirements for this interaction to take place were found to be narrow and very specific. Only two model complexes, **1-Co** and **7-Co**, form a hydrogen bond to bound dioxygen, which was characterized in terms of geometry and nature of the bond. The geometry and dipolar nature of this interaction in **1-Co**-$O_2$ is more similar to the one in natural cobalt myoglobin (Co-Mb), making **1-Co** the best model compound in the entire series.

**Keywords:** ENDOR spectroscopy · heme proteins · hydrogen bonds · molecular recognition · porphyrinoids

## Introduction

The active sites of a number of important heme proteins—including myoglobin (Mb),[1] hemoglobin (Hb),[2] or peroxidases (PO)[3]—consist of a prosthetic heme group, which is axially coordinated by a proximal histidine residue and contain a second, distal histidine which can serve as a hydrogen-bond donor to bound ligands. Recently, we reported on a proper pulse EPR method to directly measure hydrogen bonding between the distal side residue and bound dioxygen in Co-Mb-$O_2$ and in the model compound **1-Co**-$O_2$.[4] The complete analysis of the hyperfine splitting caused by the hydrogen bond in **1-Co**-$O_2$ allowed for the determination of the distance between bound $O_2$ and the interacting proton as well as the characterization of the nature of this interaction, which was found to be dominated by a dipolar contribution.[4]

In the present study, we describe the synthesis of a series of related model porphyrins **2-Co** to **5-Co**, bearing different distal residues, and examine the hydrogen-bonding properties towards bound dioxygen. We also included the earlier reported complex **1-Co**[4] and the two dendritic model systems **6-Co** and **7-Co** in this investigation.[5] For the complexes **1-Co** to **5-Co**, an alkyl-tethered imidazole is used as mimic for the proximal histidine in the protein, whereas for complexes **6-Co** and **7-Co** 1,2-dimethylimidazole (DiMeIm) acts as external axial base. An alkyne-appended residue serves as explicit hydrogen-bond donor in our model compounds to simulate the function of the distal histidine in the natural proteins. We chose two benzimidazole regioisomers (in **1-Co** and **3-Co**), imidazole (**2-Co**), indole (**4-Co**), benzyl alcohol (**6-Co**), and benzamide (**7-Co**), while methylated benzimidazole (**5-Co**), incapable of acting as hydrogen-bond donor, was used as negative control. Only the distal hydrogen-bond donating proton is exchangeable by $D_2O$ in complexes **1-Co** to **4-Co**, **6-Co**, and **7-Co**. The structural representations of compounds **1-Co** to **5-Co**, **6-Co**-DiMeIm, and **7-Co**-DiMeIm are shown in Figure 1.

[a] Dr. H. Dube, Dr. B. Felber, Dr. M. Saito, Prof. Dr. F. Diederich
Laboratorium für Organische Chemie, ETH Zurich
Hönggerberg, HCI, 8093 Zurich (Switzerland)
Fax: (+41) 44-632-1109
E-mail: diederich@org.chem.ethz.ch

[b] B. Kasumaj, Dr. C. Calle, Prof. Dr. G. Jeschke
Laboratorium für Physikalische Chemie, ETH Zurich
Hönggerberg, HCI, 8093 Zurich (Switzerland)
Fax: (+41) 44-632-1021
E-mail: gunnar.jeschke@phys.chem.ethz.ch

Supporting information for this article is available on the WWW under http://dx.doi.org/10.1002/chem.200802077.

 © 2009 Wiley-VCH Verlag GmbH & Co. KGaA, Weinheim WILEY InterScience DISCOVER SOMETHING GREAT 

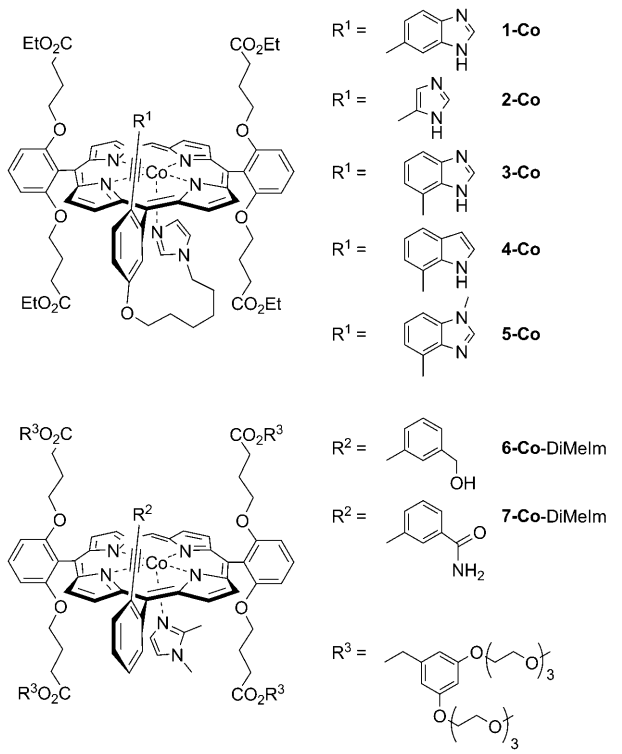


Figure 1. Chemical structures of model compounds **1-Co** to **5-Co** and **6-Co**-DiMeIm and **7-Co**-DiMeIm for the active sites of Mb, Hb, or PO.

## Results and Discussion

**Modeling**: Detailed conformational analyses at the semiempirical PM5 level of theory were performed for the dioxygen adducts of the (for easier modeling) $Fe^{II}$ complexes **1-Fe**-$O_2$ to **3-Fe**-$O_2$, and at the PM3 level of theory for **7-Fe**-(DiMeIm)($O_2$), prior to synthesis, using the MOPAC 2002 package[6] (see Supporting Information). In complexes **1-Fe**-$O_2$ and **7-Fe**-(DiMeIm)($O_2$) the interacting NH proton of the distal residues was found to be located at longer distances from bound dioxygen ($d_{NH\cdots O\text{-}O}=2.44$ and $d_{NH\cdots O\text{-}Fe}=3.30$ Å for **1-Fe**-$O_2$ and $d_{NH\cdots O\text{-}O}=2.37$ and $d_{NH\cdots O\text{-}Fe}=2.76$ Å for **7-Fe**-(DiMeIm)($O_2$)), compared with Mb-$O_2$ (1.98 and 2.44 Å).[7] In derivatives **2-Fe**-$O_2$ and **3-Fe**-$O_2$, with imidazole and 7-substituted benzimidazole, respectively, as distal residues, the corresponding values are considerably smaller (1.34 and 2.23 Å; and 1.35 and 2.21 Å, respectively) leading to stronger hydrogen bonding in the modeling of these complexes.

**Synthesis**: The model complexes **2-Co** to **5-Co** were synthesized via a porphyrin condensation reaction using substituted dipyrromethane **8**, unsubstituted dipyrromethane **9**,[8] and aldehyde **10**[9] (Scheme 1).

Dipyrromethane **8** was obtained in two steps from 2-bromo-5-hydroxybenzaldehyde (**11**).[10] Sonogashira cross-coupling of **11** with *i*$Pr_3$Si-acetylene using [$Pd(PPh_3)_4$] as catalyst together with CuI afforded the desired coupling product **12** in 90% yield (Scheme 2). The condensation of **12** with pyrrole under acid catalysis furnished the substituted dipyrromethane **8** in 79% yield. The three-step synthesis of aldehyde **10** has been described earlier.[9] However, changing to $CH_2Cl_2$ as solvent and $AlCl_3$ as Lewis acid for the deprotection of the precursor 1,6-dimethoxybenzaldehyde (**13**) gives rise to higher yield and easier purification of the resulting 1,6-dihydroxybenzaldehyde (**14**) compared to the previous protocol.

The porphyrin synthesis (Scheme 1) proceeded in two steps, condensation of the dipyrromethanes **8** and **9** with aldehyde **10** under TFA catalysis and consecutively aromatization of the macrocycle with chloranil, as described previously.[4] Zinc ions were inserted into the obtained free-base porphyrin **15-2H** to yield the corresponding complex **15-Zn** to which 1-(6-bromohexyl)imidazole (**16**)[11] was attached to yield **17-Zn**. After removal of the *i*$Pr_3$Si group, porphyrin **18-Zn** was obtained in 93% yield.

The different distal residues were attached by means of Sonogashira cross-coupling reactions (Scheme 1). The syntheses of the iodinated precursors 4,5-iodoimidazole (**19**),[12] 4,7-iodobenzimidazole (**20**),[13] and 7-iodoindole (**21**),[14] are described in the literature. Conversion of triazene **22**, which was prepared in high yield from the corresponding amine **23**,[15] into 4,7-iodobenzimidazole (**20**) was accomplished in much higher yield (71%) compared to the published protocols (10%)[13] as shown in Scheme 3. 1-Methyl-4-iodobenzimidazole (**24**) was prepared from **20** by using neat dimethyl carbonate (DMC) and DBU as base. The selective methylation was confirmed by NOE from the proton at C(4) towards the methyl group.

Attachment of the different distal residues was postponed towards the end of the synthesis to facilitate easy modification of the "distal site" without changing the whole synthetic sequence. The attachment of the different hydrogen-bond donors **19** to **21** and **24** to the porphyrin precursor **18-Zn** was achieved in satisfactory yields, leading to porphyrins **2-Zn** to **5-Zn** (Scheme 1). After the $Zn^{II}$ ion was removed with TFA, $Co^{II}$ was inserted into the intermediate free-base porphyrins using $CoCl_2$ (Scheme 1). In the case of **2-Co**, **3-Co**, and **5-Co**, $Co^{II}$ insertion provided a mixture of both $Co^{II}$ and $Co^{III}$ porphyrins as was apparent from their UV/Vis spectra.[16] Therefore, an additional reduction with an aqueous solution of sodium dithionite was performed, affording predominantly the $Co^{II}$-containing complexes.

**Conformation of the zinc complexes in solution**: For complexes **17-Zn** ($CDCl_3$), **18-Zn** ($CDCl_3$), **1-Zn**, and **3-Zn** to **5-Zn** ($CDCl_3$ and $CD_2Cl_2$) the $^1$H NMR resonances of the alkyl-tethered imidazole are significantly shifted upfield, indicative of axial ligation to the $Zn^{II}$ ion.[11] In Figure 2, the $^1$H NMR spectrum of **3-Zn** in $CDCl_3$ is shown exemplarily. In sharp contrast, these upfield shifted signals were lacking in the $^1$H NMR spectrum of **2-Zn** ($CDCl_3$ and $CD_2Cl_2$), indicating that the distal alkyne-appended imidazole competes with the alkyl-tethered imidazole as fifth axial ligand to the $Zn^{II}$ ion. A similar effect on the upfield shifted signals was observed upon adding an external nitrogen base to a solu-

 © 2009 Wiley-VCH Verlag GmbH & Co. KGaA, Weinheim 

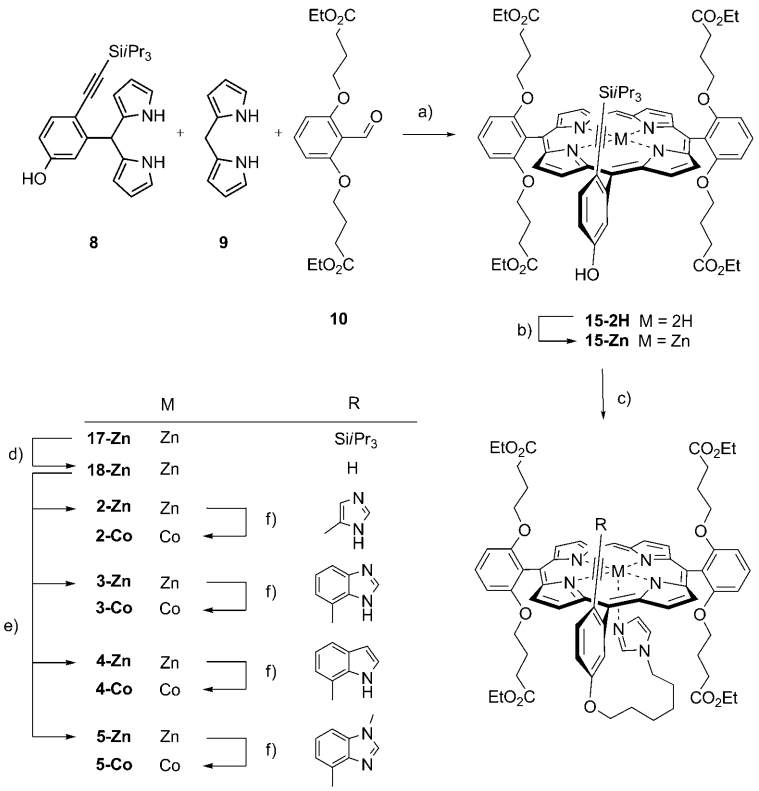


Scheme 1. Synthesis of the model compounds **2-Co** to **5-Co**. a) TFA, $CH_2Cl_2$, 20 °C, 16 h, then chloranil, 40 °C, 2 h, 15 %; b) $Zn(OAc)_2{\cdot}2H_2O$, MeOH/$CHCl_3$, 65 °C, 1 h, 96 %; c) 1-(6-Bromohexyl)imidazole (**16**), $Cs_2CO_3$, DMF, 20 °C, 14 h, 79 %; d) $n$Bu$_4$NF, THF, 20 °C, 40 min, 93 %; e) iodinated precursors **19** to **21** and **24**, [Pd($PPh_3$)$_4$], CuI, $NEt_3$, DMF, 100 °C, 4 h, 48 %–74 %; f) 1) TFA, $CHCl_3$, 20 °C, 12 min, quant.; 2) $CoCl_2$, 2,6-lutidine, THF, 20 °C, 12 h. TFA = trifluoroacetic acid.

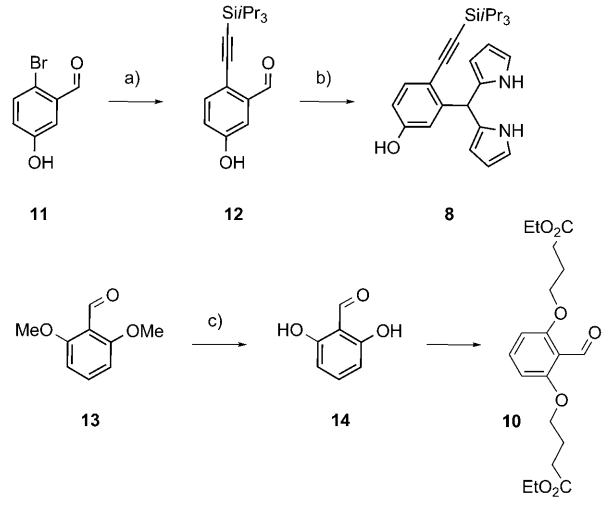


Scheme 2. Synthesis of the precursor molecules **8** and **10**. a) $i$Pr$_3$Si-acetylene, [Pd($PPh_3$)$_4$], CuI, $NEt_3$, 80 °C, 12 h, 90 %; b) pyrrole, TFA, 20 °C, 10 min, 79 %; c) $AlCl_3$, $CH_2Cl_2$, 20 °C, 12 h, 87 %.

tion of compound **3-Zn** ($CDCl_3$). Addition of only 0.25 equivalents of 1-methylimidazole (1-MeIm) leads to pronounced peak broadening and weakening especially for the upfield shifted proton signals of the alkyl-tethered imidazole (Figure 2c). Thus, an external nitrogen base can significantly compete with the intramolecular binding of the alkyl-tethered imidazole in our complexes.

In porphyrins **1-Zn** to **3-Zn**, the NH proton of the distal residue was readily exchanged by deuterium within seconds using $D_2O$ (Figure 2b). The $D_2O$ exchange for **7-Co** was tested with 3-iodobenzamide, and was complete after 4 h. HSQC (heteronuclear single quantum coherence) and HMBC (heteronuclear multiple bond correlation) NMR allowed for direct assignment of almost all proton resonances for complexes **3-Zn** and **4-Zn**. Distinct upfield shifted signals revealed the distal residues in both complexes to be positioned with their NH proton directly above the porphyrin plane. Such conformation presumably is strongly preferred due to efficient N-H···π interactions with the porphyrin chromophore.[17] Accordingly,

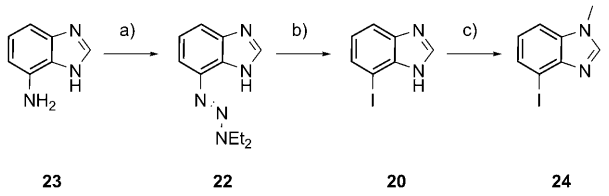


Scheme 3. Synthesis of iodinated benzimidazoles **20** and **24**. a) 1) HCl conc., THF, $Et_2O$, MeCN, 0 °C, 30 min, 2) $NaNO_2$, $H_2O$, 0 °C, 40 min, 3) $K_2CO_3$, $NEt_2H$, $H_2O$, MeCN, 0 to 20 °C, 12 h, 94 %; b) NaI, $Me_3SiCl$, MeCN, 20 °C, 12 h, 71 %, c) DBU, DMC, 90 °C, 15 h, 72 %. DBU = 1,8-diazabicyclo[5.4.0]undec-7-ene, DMC = dimethyl carbonate.

there is only one tautomeric form of the distal benzimidazole in **3-Zn** present in solution.

The situation is similar in complex **1-Zn**, although its $^1$H NMR spectrum shows broadened peaks. Still the upfield shifts of the alkyl-tethered imidazole protons as well as of the $D_2O$ exchangeable distal NH proton are clearly visible (see Supporting Information of ref. [4]). Except for the $D_2O$-exchangeable NH proton, which is also upfield shifted, the corresponding signals are, however, not visible in the $^1$H NMR spectrum of **2-Zn**. The signal of the NH proton is not affected and thus, the NH proton does not seem to par-

 © 2009 Wiley-VCH Verlag GmbH & Co. KGaA, Weinheim 

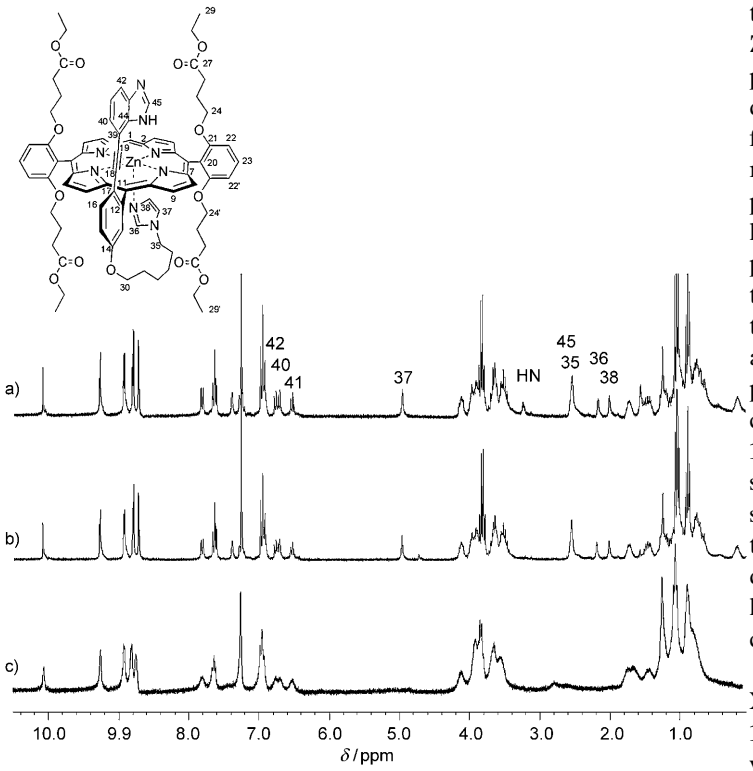


Figure 2. 300 MHz $^1$H NMR spectra of **3-Zn** in $CDCl_3$ at 20°C. a) Before and b) after $D_2O$ exchange, c) after adding 0.25 equiv 1-MeIm. Indicative proton resonances are marked. The NH proton signal disappears after $D_2O$ exchange. The resonances of the alkyl-tethered axial imidazole disappear upon addition of 1-MeIm.

ticipate in any tautomerization equilibrium in complex **2-Zn**. Again, its upfield shift indicates proximity to the porphyrin plane. For complex **5-Zn** ($CDCl_3$ and $CD_2Cl_2$), the distal methylated benzimidazole is rotated outwards, away from the porphyrin plane, presumably because of electronic repulsion between the benzimidazole *N*-lone pair and the porphyrin π-cloud. Complexes **6-2H** and **7-2H** ($CDCl_3$) also have their distal residues positioned above the porphyrin plane as can be seen from the indicative upfield shifts of their proton signals.[5] Again, attractive interactions between the exchangeable distal protons and the porphyrin π-cloud are most likely responsible for the observed conformational preferences in complexes **6-2H** and **7-2H**.[17] The preferred conformations of distal and proximal residues in complexes **1-Zn** to **5-Zn** as well as in **6-2H** and **7-2H** in solution are summarized in Figure 3 together with indicative chemical shifts of the pertinent $^1$H NMR resonances. After this detailed conformational analysis, we were confident that the different distal residues were indeed suitable for effective hydrogen bonding to bound dioxygen in the corresponding cobalt complexes.

**X-band continuous wave (CW) EPR spectroscopy**: Complex **1-Co** was measured in $CH_2Cl_2$, $CD_2Cl_2$, and toluene as solvent, complex **3-Co** in $CHCl_3$ as solvent, complexes **2-Co**, **4-Co** and **5-Co** were measured in $CH_2Cl_2$ as solvent, and complexes **6-Co**-DiMeIm, and **7-Co**-DiMeIm were measured in toluene as solvent. The CW EPR spectra of all $Co^{II}$ complexes exhibit the common features of a low-spin $Co^{II}$ species with dominating $d_{z^2}$ character in a porphyrin environment as shown exemplarily for **2-Co** in Figure 4.

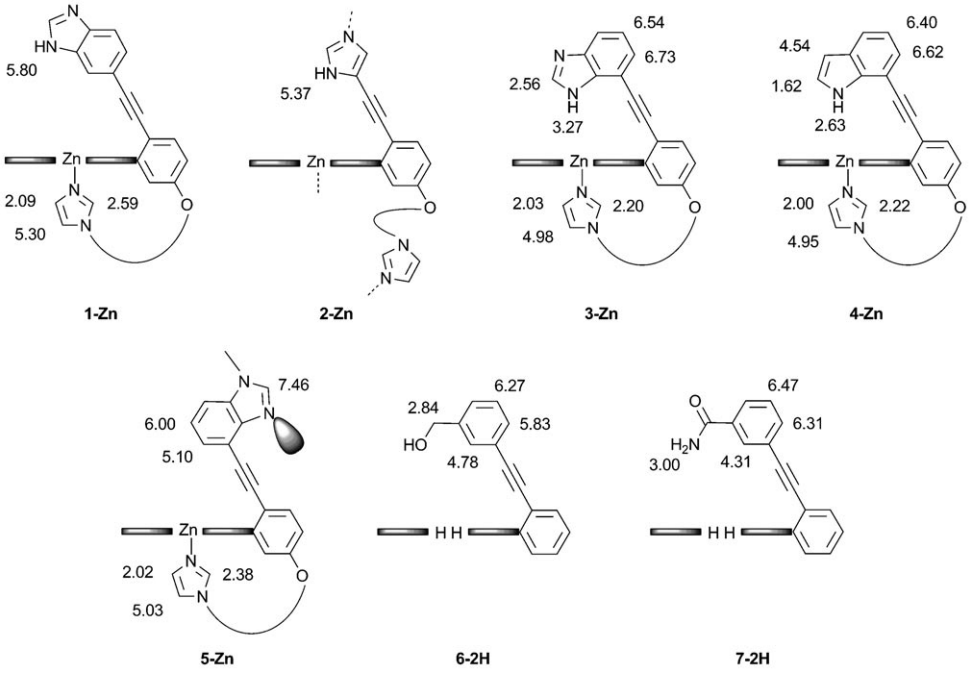


Figure 3. Schematic view of the preferred conformations of model complexes **1-Zn** to **7-Zn** in solution ($CDCl_3$ at 20°C) as determined by NMR spectroscopy. Indicative proton signal shifts are given in ppm. Certain residues of the molecules were omitted for clarity.

 © 2009 Wiley-VCH Verlag GmbH & Co. KGaA, Weinheim 

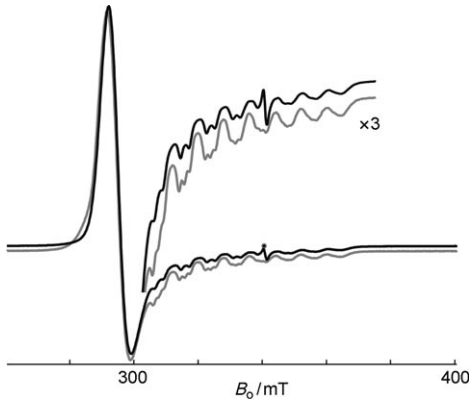


Figure 4. X-band CW EPR spectra of **2-Co** with alkyl-tethered $^{14}$N-imidazole as axial base (grey) resulting in a triplet hyperfine splitting and **$^{15}$N-2-Co** with alkyl-tethered $^{15}$N-imidazole as axial base (black) resulting in a doublet hyperfine splitting. Spectra were measured in $CH_2Cl_2$ at 120 K. * Radical contamination.

The axial symmetry of the obtained spectra indicates the absence of severe geometric distortions of the complexes. Similar spectra were obtained from $Co^{II}$-Mb.[4] A triplet hyperfine splitting arises from the presence of the axial nitrogen base. However, in complex **2-Co** it was not yet apparent which of the two imidazoles was bound to the $Co^{II}$ ion, given the ligation situation in **2-Zn**. To resolve the ambiguity, the alkyl-tethered imidazole was exchanged by its bis-$^{15}$N-labeled analogue in **2-Co**. A doublet hyperfine splitting was observed in the corresponding CW EPR spectrum, proving that only the alkyl-tethered imidazole serves as axial ligand in **2-Co** (Figure 4).

Dioxygen adducts were obtained within seconds by exposing samples of **1-Co** to **3-Co** and **5-Co** to dioxygen and **6-Co**-DiMeIm, and **7-Co**-DiMeIm to air at 20 °C. Considerable formation of a dioxygen adduct of **4-Co** could not be observed even under forcing conditions (up to 40 °C and 4 bar dioxygen pressure). We assume that the distal indole NH undergoes strong N-H···π interactions with the porphyrin π-system, leaving no space for dioxygen binding in this complex. Similar to **5-Zn**, complex **5-Co** is expected to rotate its distal methylated benzimidazole moiety outwards—away from the porphyrin plane—since its free electron pair would be repelled by the π-cloud of the macrocycle. This rotamer provides a less hindered coordination site, allowing for dioxygen binding in this complex. Apparently, in complex **3-Co** a similar rotation permits dioxygen to bind.

By forming the dioxygen adducts, the spin population is transferred from the central ion to the attached dioxygen nuclei. This results in a different X-band CW EPR spectrum, exhibiting more narrow features (see Supporting Information). Similar X-band CW EPR spectra are found for dioxygen adducts of $Co^{II}$-Mb.[4]

**Pulse EPR spectroscopy**: In order to minimize peak overlapping and cross suppression,[18] the following pulse EPR experiments were conducted at higher excitation frequencies (Q-band). First, field-swept FID-integral-detected EPR spectra were recorded to determine the magnetic field (observer) positions for the pulse EPR experiments. Subsequently, the dioxygen adducts **1-Co**-$O_2$ to **3-Co**-$O_2$, **5-Co**-$O_2$, **6-Co**-(DiMeIm)($O_2$), and **7-Co**-(DiMeIm)($O_2$) were studied by Q-band Davies-ENDOR (electron nuclear double resonance) spectroscopy[19] in order to determine the hyperfine interactions caused by protons close to bound dioxygen. For complex **1-Co**-$O_2$, the largest proton hyperfine coupling—ranging from 5.0 to 14.0 MHz—disappeared upon $D_2O$ exchange as reported earlier.[4] Two different preparation pulse lengths (160 and 80 ns) were applied for the complete detection of the splitting, since shorter preparation pulse lengths enhance the relative intensity of larger hyperfine splittings.[19a] The geometry and nature of that hydrogen bond was fully analyzed by means of simulations and additional HYSCORE measurements.

A large hyperfine splitting, similar to the one observed for **1-Co**-$O_2$, was not found in the spectra of **2-Co**-$O_2$, **3-Co**-$O_2$, **5-Co**-$O_2$, and **6-Co**-(DiMeIm)($O_2$) (spectra are shown in the Supporting Information). Moreover, upon $D_2O$ exchange, no significant change could be observed in the spectra of complex **3-Co**-$O_2$. Thus, a hydrogen-bond interaction of bound dioxygen with a nearby exchangeable proton was precluded in these complexes. Due to the reduction step following the $Co^{II}$ insertion the organic solvent was water-saturated. The lack of any strong and $D_2O$ exchangeable interaction in these complexes shows that also residual solvent water is not forming hydrogen bonds towards dioxygen.

Our negative control **5-Co**-$O_2$ does not possess a distal proton capable of hydrogen bonding, and therefore it was expected not to show a significantly large hyperfine splitting. As we argued above, rotation of the distal residue away from the porphyrin macrocycle allows for the formation of a dioxygen adduct of complexes **3-Co** and **5-Co**. In this conformation, a hydrogen-bond interaction cannot be formed between the distal benzimidazole NH proton and bound dioxygen in **3-Co**-$O_2$, which is the reason for the lack of a large hyperfine interaction.

Also in complex **2-Co**-$O_2$, no hydrogen-bond interaction was found although the NH proton is expected to be very close to bound dioxygen based on the prior modeling. The dioxygen adduct formation proceeded by far the fastest for **2-Co** in comparison to the other model compounds but was accompanied by significant signal decrease indicating substantial irreversible oxidation. We assume that a proton transfer from the distal imidazole and consecutively very fast irreversible oxidation of the $Co^{II}$ ion takes place, similar to natural autoxidation processes.[20] Most likely, only dioxygen adducts of **2-Co**-$O_2$ lacking an interaction with the distal imidazole NH proton were isolated in our experimental setup. We conclude, that the distal imidazole residue in **2-Co** actually is a too good hydrogen-bond donor and does not stabilize bound dioxygen but rather activates it for irreversible oxidation.

The dioxygen adduct of complex **6-Co**-DiMeIm bearing a benzyl alcohol as the distal residue also did not show a large hyperfine splitting in the Davies-ENDOR spectra and an

 © 2009 Wiley-VCH Verlag GmbH & Co. KGaA, Weinheim 

operative hydrogen bond had to be excluded in this complex. In benzyl alcohols, the torsional angle C($sp^2$)-C($sp^2$)-C($sp^3$)-O prefers values around 90°, thereby orienting the HO-group perpendicular to the benzene plane. This conformational preference could impede proper hydrogen bonding in **6-Co**-(DiMeIm)($O_2$) by moving the distal OH-group away from bound dioxygen.

In the modeling of complex **7-Fe**-(DiMeIm)($O_2$), slightly shorter distances for a distal hydrogen bond as compared to complex **1-Fe**-$O_2$ were obtained. Hence, we expected a similar hydrogen bond in **7-Co**-(DiMeIm)($O_2$). We were delighted to observe indeed a very large hyperfine splitting in the Davies-ENDOR spectra of **7-Co**-(DiMeIm)($O_2$). This hyperfine splitting was also exchangeable by $D_2O$ (Figure 5a), only longer deuteration times were needed (4 h) compared to **1-Co** to **3-Co**, as the NH protons of amides are generally slower to exchange as compared to the NH protons of benzimidazoles or imidazoles. The obtained Davies-ENDOR spectra of **7-Co**-(DiMeIm)($O_2$) show the largest extension of the exchangeable hyperfine splitting close to $g_x$ and smaller extensions close to $g_y$ and $g_z$.

In order to determine whether the hyperfine matrix of the exchangeable proton has both, positive and negative principal values, the X-band 6-pulse HYSCORE[21] spectrum of **7-Co**-(DiMeIm)($O_2$) was measured close to $g_x$. Although the 6-pulse HYSCORE spectrum did not allow for measuring the full exchangeable splitting, its off antidiagonal ridge is clearly visible (Figure 6). This spectrum proves that both, positive and negative principal values exist and shows that the hyperfine coupling associated with the hydrogen bond is dominated by a through-space contribution with only a small isotropic contribution. Thus, the hydrogen bond in **7-Co**-(DiMeIm)($O_2$) is mainly ionic (dipolar) in character with only small covalent contributions, similar to the situation in **1-Co**-$O_2$ and Co-Mb-$O_2$.[4] However, that does not exclude bonding overlap between orbitals of the two molecules to some extent. This overlap can be interpreted as a covalent contribution and can be characterized by EPR spectroscopy via the isotropic part (Fermi contact interaction) of the hyperfine coupling. Although the covalent contribution to the binding energy may be much smaller than the dipolar one, characterization of this overlap is of interest, as it is related to the ease of electron transfer between the two molecules.

Simulations of CW EPR and ENDOR spectra of **7-Co**-(DiMeIm)($O_2$) were carried out in order to derive geometry parameters and bonding properties of the exchangeable proton. The CW EPR spectra simulations of **7-Co**-(DiMeIm)($O_2$) were performed with $g=[2.0029\pm0.0005,\ 1.989\pm0.001,\ 2.0725\pm0.0001]$, the principal values of the metal hyperfine tensor $A^{Co}=[-55,\ -27,\ -26]$ MHz $\pm$ 2 MHz and a set of Euler angles ($0\pm10°$, $70\pm10°$, $0\pm20°$) with respect to the $g$ frame. Subsequently, Davies-ENDOR simulations were carried out at each field position, to fit the experimental difference spectra of protonated and deuterated **7-Co**-(DiMeIm)($O_2$) as shown in Figure 5b. We obtained a hyperfine tensor for the exchangeable proton of $A^{H}=[-5.4,\ -5.3,\ 12.5]$ MHz $\pm$ 0.5 MHz, with Euler angles of (0, 110, 0) $\pm$ 10°. The spin density was assumed to be centered at one point in space,[22] and a distance of 2.4 ($\pm$0.1 Å) between this spin density center and the NH proton of the distal benzamide was obtained by using the point-dipole approximation with a dipolar contribution $T=6.0$ MHz.[23] The hydrogen-bond geometry in **7-Co**-(DiMeIm)($O_2$) is depicted schematically in Figure 7.

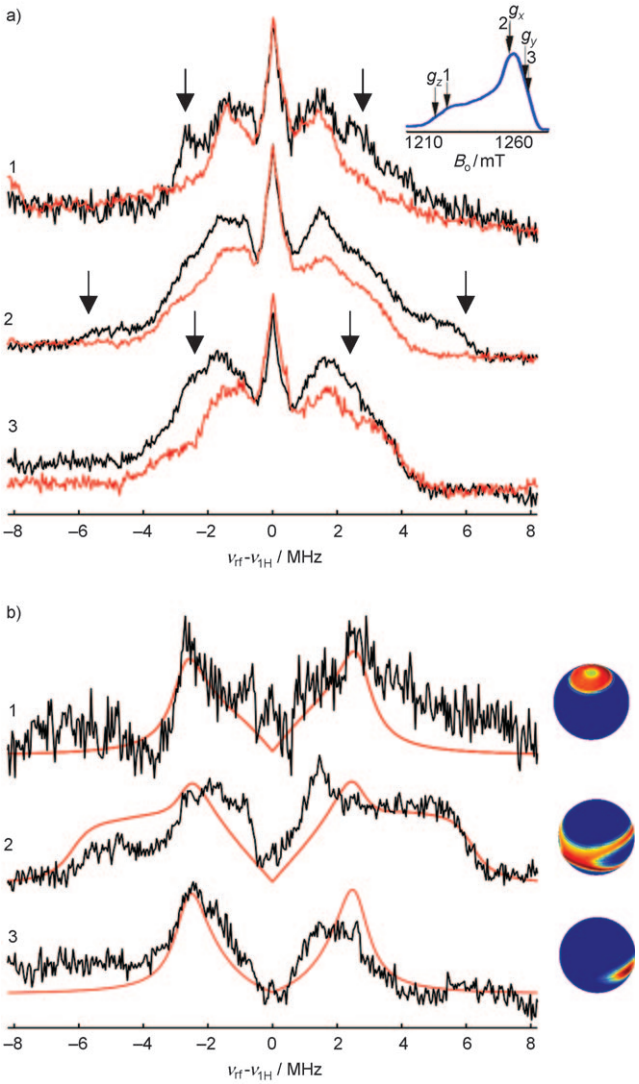


Figure 5. a) Frozen-solution (toluene) Davies ENDOR spectra of **7-Co**-(DiMeIm)($O_2$) recorded at Q-band frequency at 10 K before (black), and after $D_2O$ exchange (red). Observer positions are indicated in the inset showing the FID-integral-detected EPR spectra. A preparation pulse length of 80 ns was used. b) Corresponding difference spectra before and after $D_2O$ exchange at three different observer positions (black) and simulated spectra of the exchangeable proton (red). The orientations contributing to the experimental spectra are projected on the unit spheres.

The Davies-ENDOR spectra obtained for **7-Co**-(DiMeIm)($O_2$) show striking similarity in the evolution of the largest and exchangeable hyperfine splitting over the different magnetic field positions compared to the spectra obtained for **1-Co**-$O_2$ and natural Co-Mb-$O_2$, as shown in Figure 8. In all three dioxygen complexes the greatest exten-


© 2009 Wiley-VCH Verlag GmbH & Co. KGaA, Weinheim

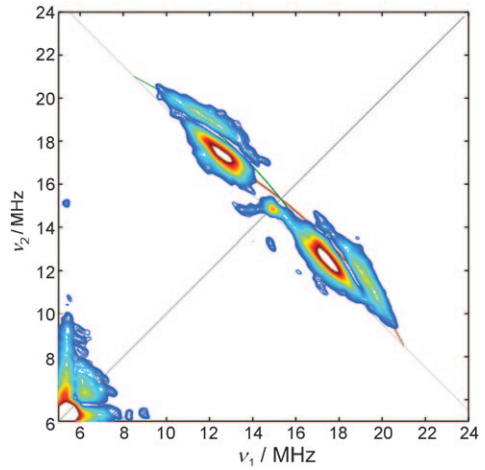


Figure 6. X-band frozen-solution 6-Pulse HYSCORE spectrum of **7-Co**-(DiMeIm)($O_2$) in toluene at 20 K at $g=2.018$. The off antidiagonal ridges stemming from the largest and exchangeable proton hyperfine splitting can clearly be distinguished from the residual antidiagonal proton splittings. The simulated ridges (green and brown line) show the signal extension expected if the modulation depth were the same for all orientations. The simulation parameters were $[g_x, g_y, g_z]=[2.0029\pm0.0005,\ 1.989\pm0.001,\ 2.0725\pm0.0005]$ and $A^H=[-5.4, -5.3, 12.5]$ MHz.

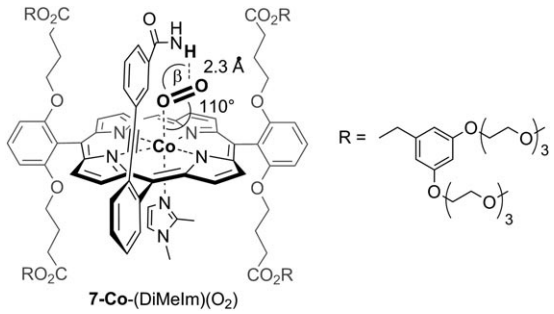


Figure 7. A distal hydrogen bond to bound dioxygen is formed in complex **7-Co**-(DiMeIm)($O_2$). The angles and distance shown were obtained from the frozen-solution EPR measurements with $\beta=110°$.

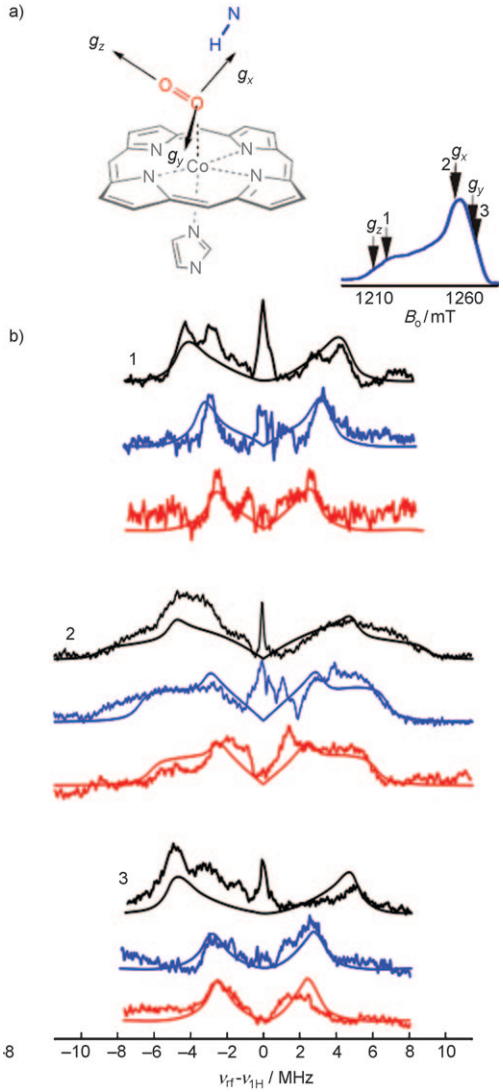


Figure 8. Comparison of the distal hydrogen bonding in **1-Co**-$O_2$, **7-Co**-(DiMeIm)($O_2$), and Co-Mb-$O_2$. a) Qualitative geometry of the distal hydrogen bond derived from experimental EPR data. b) Smoothed difference Davies-ENDOR spectra before and after $D_2O$ exchange of Co-Mb-$O_2$ (black), **1-Co**-$O_2$ (blue), and **7-Co**-(DiMeIm)($O_2$) (red) at three different observer positions close to $g_z$ (1), $g_x$ (2), and $g_y$ (3) shown together with their simulations. For simulation parameters of **1-Co**-$O_2$ and Co-Mb-$O_2$ see also ref. [4].

sion of this splitting is close to $g_x$ and thus, the N–H axis of the distal hydrogen-bond donor is virtually parallel to $g_x$. The distal hydrogen-bonded proton is positioned above the dioxygen in each case (Figure 8).

The error of the Euler angles leaves some uncertainty in $g_y$ and $g_z$ direction for the distal hydrogen-bonded proton, but again the natural protein and the two model complexes show the same tendency of having considerably weaker interactions in these directions. Therefore, the interacting distal proton cannot be situated aside or in the front or back of bound dioxygen. The hyperfine splitting caused by the distal hydrogen bond in Co-Mb-$O_2$ has the largest absolute values (up to 19 MHz), and, correspondingly, the hydrogen bond length is the shortest in the natural protein (≈2.0 Å). The hyperfine splittings caused by the distal hydrogen bonds in the two model complexes **1-Co**-$O_2$ and **7-Co**-(DiMeIm)($O_2$) are similar to each other and smaller (up to 14 MHz) corresponding to a longer hydrogen bond (≈2.3 and ≈2.4 Å, respectively). The hyperfine splittings of the exchangeable proton in **1-Co**-$O_2$ are slightly larger compared to **7-Co**-(DiMeIm)($O_2$) especially close to $g_z$ (Figure 8). All three hydrogen-bond interactions are essentially dipolar in nature with only little covalent contribution. Thus, like **1-Co**, also **7-Co**-DiMeIm is a very good, functional model for the natural proteins Mb and Hb, reproducing very well the distal interactions.

 © 2009 Wiley-VCH Verlag GmbH & Co. KGaA, Weinheim 

## Conclusion

We discussed in this paper the delicate dependence of distal hydrogen-bond formation towards bound dioxygen on the proper geometry of the interacting distal residue. A series of new model complexes for dioxygen binding heme proteins were analyzed in terms of their distal hydrogen bonding. Our synthetic model system allowed us to change the distal hydrogen bond donor in a very controlled fashion and study the direct effect of these changes. The model complexes **1-Co** and **7-Co** were found to possess ideal distal constitution to form hydrogen bond interactions with bound dioxygen. The distal hydrogen bonding in their corresponding dioxygen adducts is similar in geometry and dipolar nature to the hydrogen bond in natural Co-Mb-$O_2$. Therefore, both complexes can be regarded as very good functional models for the dioxygen binding sites of Mb and Hb. All other complexes studied did not show distal hydrogen bonding towards bound dioxygen, suggesting that the geometry requirements for this interaction are narrow and very specific. The similarity of the hydrogen bonding in **1-Co**, **7-Co** and Co-Mb supports this conclusion and gives quantitative insight into the geometrical prerequisites for this interaction to take place.

## Experimental Section

**Materials and general methods**: Reagents and solvents were purchased at reagent grade from Acros, Aldrich, and Fluka, and used as received. Tetrahydrofuran (THF) was freshly distilled from Na/benzophenone, $CH_2Cl_2$ from $CaH_2$ under $N_2$, and *N*,*N*-dimethylformamide (DMF) was purchased from Fluka ($[H_2O] < 0.005\,\%$). $NEt_3$ was freshly distilled from $CaCl_2$. All cross-coupling reactions were performed under an inert atmosphere by applying a positive pressure of $N_2$ or Ar. Freshly dried solvents for the glove box experiments were carefully degassed by at least four freeze–pump–thaw cycles ($1\times10^{-3}$ mbar). Compounds dipyrrylmethane **9**,[8] aldehyde **10**,[9] 2-bromo-5-hydroxbenzaldehyde (**11**),[10] aldehyde **13**,[9] 1-(6-bromohexyl)imidazole (**16**),[11] porphyrins **15-2H**; **15-Zn**, **17-Zn**, and **18-Zn**,[4] 4(5)-iodoimidazole (**19**),[12] 7-iodoindole (**21**),[14] and 4(7)-aminobenzimidazole (**23**)[15] were synthesized according to literature procedures. Column chromatography (CC) was carried out with $SiO_2$ 60 (particle size 0.040–0.063 mm, 230–400 mesh; Fluka) or $Al_2O_3$ (Alumina N, Akt. I, ICN Biomedicals GmbH) and distilled technical solvents. Gel permeation chromatography (GPC) was carried out using a glass column (4.5× 300 cm) with Bio-Rad Bio-Beads S-X1, elution with THF (stabilized, Fluka) at 20 °C operated by gravity. Thin-layer chromatography (TLC) was conducted on glass plates coated with $SiO_2$ 60 $F_{254}$ obtained from Merck; visualization with a UV lamp (254 or 366 nm). Melting points (m.p.) were measured on a Büchi B-540 melting point apparatus in open capillaries and are uncorrected. "Decomp" refers to decomposition. $^1$H NMR and $^{13}$C NMR spectra were measured on a Varian Gemini 300 or on a Bruker DRX500 spectrometer at 20 °C unless otherwise stated. Chemical shifts ($\delta$) are reported in ppm relative to the signal of tetramethylsilane (TMS). Residual solvent signals in the $^1$H and $^{13}$C NMR spectra were used as an internal reference ($CDCl_3$: $\delta_H = 7.263$, $\delta_C = 77.0$ ppm; $CD_2Cl_2$: $\delta_H = 5.32$, $\delta_C = 53.8$ ppm). Coupling constants ($J$) are given in Hz. The apparent resonance multiplicity is described as s (singlet), b (broad signal), d (doublet), t (triplet), q (quartet), and m (multiplet). All NMR signals that can be assigned with certainty are identified in the experimental details according to the arbitrary numbering used in Figure 2. The proton signals of the different distal residues are assigned descriptively. Infrared spectra (IR) were recorded on a Perkin-Elmer FT1600; absorption bands are reported by wavenumber ($cm^{-1}$), signal designations: vs (very strong), s (strong), m (medium), w (weak). UV/Vis spectra were recorded on a Varian Cary-5 spectrophotometer. The spectra were measured in $CHCl_3$ or $CH_2Cl_2$ in a quartz cuvette (1 cm) or an air-tight cuvette in case of the cobalt complexes at 20 °C. The absorption wavelengths ($\lambda$) are reported in nm with the extinction coefficient ($\varepsilon$) $M^{-1}\,cm^{-1}$ in brackets; shoulders are indicated as sh. HR Electron Impact (HR-EI) mass spectra were measured on a Micromass AutoSpec-Ultima spectrometer, Electronspray Ionization (ESI) mass spectra were measured on a Finnigan TSQ-7000 spectrometer, high-resolution (HR) FT-ICR-MALDI spectra were measured on an IonSpec Ultima Fourier transform (FT) instrument with [(2*E*)-3-(4-*tert*-butylphenyl)-2-methylprop-2-enylidene]malononitrile (DCTB), or 3-hydroxypicolinic acid (3-HPA) as the matrix. The most important peaks are reported in $m/z$ units with $[M]$ as the molecular ion. MALDI-TOF spectra were recorded on a Bruker Daltonics Ultraflex mass spectrometer using DCTB as matrix. Elemental analyses were performed by the Mikrolabor at the Laboratorium fuer Organische Chemie, ETH Zurich, with a LECO CHN/900 instrument.

**EPR and ENDOR measurements**: CW EPR measurements at X-band were carried out on a Bruker E500 spectrometer equipped with a superhigh Q cavity. Experimental conditions: microwave frequency, 9.53 GHz; modulation frequency, 100 kHz; modulation amplitude, 0.2 mT. Cooling of the sample was performed with a liquid nitrogen finger Dewar ($T$= 120 K). X-band 6-pulse HYSCORE spectroscopy (microwave frequency 9.78 GHz) were performed on a Bruker E580 spectrometer at 20 K with the pulse sequence $(\pi/2)_x$–$\tau$–$(\pi)_x$–$\tau$–$(\pi/2)_y$–$T_1$–$(\pi)_y$–$T_2$–$(\pi/2)_y$–$\tau$–$(\pi)_y$–$\tau$–echo were carried out with the following instrumental parameters: nominal pulse lengths $t_{\pi/2} = 12$ ns, $t_\pi = 24$ ns; starting values of the two variable times $T_1$ and $T_2$, 48 ns; time increment $\Delta T = 16$ ns (data matrix 320× 320); $\tau = 112$ ns. An eight-step phase cycle was used to remove unwanted echoes. Pulse EPR measurements at Q-band (microwave frequency $35.25 \pm 0.05$ GHz) were performed on a home-built spectrometer[24] at 10 K. The FID-integral-detected EPR spectra were recorded directly via the FID following a weak 500 ns π pulse or via the FID following a weak 500 ns π pulse followed by a strong 40 ns π/2 pulse (1024 field positions). A two-step phase cycle was used in the latter case. Davies-ENDOR experiments were carried out with the pulse sequence π–$T$–π/2–$\tau$–π–$\tau$–echo, using a 8 μs radiofrequency pulse during the free evolution time $T$ (750 radiofrequency increments). The EPR spectra were simulated using the MATLAB-based program EasySpin,[25] developed at the Laboratory of Physical Chemistry ETH Zurich (http://www.easyspin.org).

**General procedure for the Sonogashira cross-coupling reaction used for the attachment of the distal residues**: A dry, $N_2$-flushed 10 mL Schlenk tube, equipped with a magnetic stirrer and a septum, was charged with **18-Zn** or **$^{15}$N-18-Zn** (1.0 equiv), the respective iodinated precursor **19** to **21** or **24** (4.0 equiv), CuI (1.3 equiv), and $[Pd(PPh_3)_4]$ (0.8 equiv). The Schlenk tube was carefully evacuated again and purged with $N_2$ twice. Dry DMF and $NEt_3$ (1:1.7 mixture to give a 0.01 M solution) were added, and the mixture was stirred 4 h at 100 °C under $N_2$. Saturated aqueous solutions of $NH_4Cl$ and EtOAc were added and the phases separated. The aqueous phase was extracted with EtOAc (2×), and the combined organic phases were dried ($Na_2SO_4$), filtered, and concentrated *in vacuo*. Purification by CC ($SiO_2$, $CH_2Cl_2$/MeOH 100:0 to 97:3), preparative GPC (SX-1, THF) followed again by CC (2×$SiO_2$, $CH_2Cl_2$/MeOH 100:0 to 97:3) afforded the model complexes **2-Zn** to **5-Zn** and **$^{15}$N-2-Zn** as purple solids.

**(Tetraethyl 4,4′,4″,4‴-{[10-(2-(1*H*-imidazol-5-ylethynyl)-5-{[6-(1*H*-imidazol-1-yl)hexyl]oxy}phenyl)porphyrin-5,15-diyl-κ*N*$^{21}$,κ*N*$^{22}$,κ*N*$^{23}$,κ*N*$^{24}$]bis-[benzene-2,1,3-triylbis(oxy)]}tetrabutanoato(2−))zinc (2-Zn)**: The title compound was prepared from **18-Zn** (80 mg, 0.06 mmol) according to the general procedure using iodinated precursor **19**. Yield 40 mg (48 %); m.p. 109 °C; $^1$H NMR ($CDCl_3$, 300 MHz): $\delta = 9.87$ (s, 1H; H-C(1)), 9.09 (d, $J = 4.2$ Hz, 2H; H-C(3)), 8.71 (d, $J = 4.2$ Hz, 2H; H-C(4)), 8.44 (d, $J$= 4.5 Hz, 2H; H-C(8) or H-C(9)), 8.29 (d, $J = 4.5$ Hz, 2H; H-C(9) or H-C(8)), 7.65 (t, $J = 8.3$ Hz, 2H; H-C(23)), 7.56 (s, 1H; H-C(13)), 7.16 (d, $J = 8.7$ Hz, 1H; H-C(15) or H-C(16)), 7.02 (d, $J = 8.7$ Hz, 1H; H-C(16) or H-C(15)), 6.96 (d, $J = 8.3$ Hz, 2H; H-C(22′)), 6.89 (d, $J = 8.3$ Hz, 2H; H-C(22)), 6.80 (brs, 1H; H-C(distal imidazole)), 5.37 (brs, 1H; NH), 4.00–

 © 2009 Wiley-VCH Verlag GmbH & Co. KGaA, Weinheim 

3.60 (m, 10H; $H_2$-C(24), $H_2$-C(28′), and $H_2$-C(30)), 3.50–3.28 (m, 8H; $H_2$-C(24′) and $H_2$-C(28)), 1.80–1.60 (m, 4H; $H_2$-C(26) and $H_2$-C(31)), 1.29–0.67 (m, 28H; $H_2$-C(32) to $H_2$-C(34), $H_2$-C(25), $H_2$-C(25′), $H_2$-C(26), $H_2$-C(26′), and $H_3$-C(29′)), 0.63 ppm (t, $J$=7.2 Hz, 6H; $H_3$-C(29)), three signals not visible due to signal overlap; $^{13}$C NMR ($CDCl_3$, 75 MHz): $\delta$= 173.0, 172.7, 159.4, 157.4, 151.5, 150.1, 149.3, 149.2, 148.1, 147.9, 136.8, 135.8, 131.1, 130.8, 130.3, 130.1, 129.5, 129.2, 128.3, 125.5, 124.0, 122.1, 120.0, 118.6, 116.0, 114.0, 111.2, 109.7, 105.8, 105.4, 104.9, 93.7, 77.3, 67.9, 67.5, 66.8, 60.1, 59.5, 46.8, 30.9, 29.7, 29.5, 29.0, 26.3, 25.5, 23.4, 14.2, 13.6 ppm; IR (neat): $\tilde{\nu}$=2924 (m), 2359 (w), 1725 (s), 1592 (m), 1520 (w), 1455 (s), 1373 (m), 1294 (m), 1231 (s), 1177 (s), 1089 (vs), 1056 (vs), 1029 (s), 990 (vs), 940 (m), 838 (m), 828 (m), 793 (s), 716 $cm^{-1}$ (s); UV/Vis ($CHCl_3$): $\lambda_{max}$ ($\varepsilon$)=595 (3.700), 559 (17.200), 426 (434.100), 404 nm (43.600 $M^{-1}cm^{-1}$, sh); HR-MALDI-MS (3-HPA): $m/z$: calcd for $C_{76}H_{80}N_8O_{13}Zn^+$: 1376.5131; found: 1376.5150 $[M]^+$; elemental analysis calcd (%) for $C_{81}H_{83}N_7O_{13}Zn$ (1427.98): C 68.13, H 5.86, N 6.87; found: C 68.13, H 5.97, N 6.58.

**(Tetraethyl 4,4′,4″,4‴-{[10-(2-(1*H*-imidazol-5-ylethynyl)-5-{[6-(1*H*-[1,3-$^{15}N_2$]imidazol-1-yl)hexyl]oxy}phenyl)porphyrin-5,15-diyl-κ$N^{21}$,κ$N^{22}$, κ$N^{23}$,κ$N^{24}$]bis [benzene-2,1,3-triylbis(oxy)]}tetrabutanoato(2−))zinc ($^{15}$N-2-Zn)**: The title compound was prepared from **$^{15}$N-18-Zn** (80 mg, 0.06 mmol) according to the general procedure using iodinated precursor **19**. Yield 40 mg (48%); m.p. 105–106 °C; $^1$H NMR (300 MHz, $CDCl_3$): $\delta$=9.87 (s, 1H; H-C(1)), 9.09 (d, $J$=4.2 Hz, 2H; H-C(3)), 8.70 (d, $J$= 4.2 Hz, 2H; H-C(4)), 8.44 (d, $J$=4.5 Hz, 2H; H-C(8) or H-C(9)), 8.29 (d, $J$=4.5 Hz, 2H; H-C(9) or H-C(8)), 7.65 (t, $J$=8.4 Hz, 2H; H-C(23)), 7.57 (s, 1H; H-C(13)), 7.16 (d, $J$=8.4 Hz, 1H; H-C(15) or H-C(16)), 7.02 (d, $J$=8.4 Hz, 1H; H-C(16) or H-C(15)), 6.96 (d, $J$=8.4 Hz, 2H; H-C-(22′)), 6.88 (d, $J$=8.4 Hz, 2H; H-C(22)), 6.77 (brs, 1H; H-C(distal imidazole)), 5.38 (brs, 1H; NH), 4.00–3.70 (m, 10H; $H_2$-C(24), $H_2$-C(28′), and $H_2$-C(30)), 3.54–3.24 (m, 8H; $H_2$-C(24′) and $H_2$-C(28)), 1.75–1.62 (m, 4H; $H_2$-C(26) and $H_2$-C(31)), 1.45–0.62 (m, 28H; $H_2$-C(32) to $H_2$-C(34), $H_2$-C(25), $H_2$-C(25′), $H_2$-C(26), $H_2$-C(26′), and $H_3$-C(29′)), 0.62 ppm (t, $J$= 7.2 Hz, 6H; $H_3$-C(29)), three signals not visible due to signal overlap; $^{13}$C NMR ($CDCl_3$, 75 MHz): $\delta$=173.0, 172.7, 159.3, 157.4, 150.1, 149.3, 149.2, 148.1, 147.9, 136.9, 131.1, 130.8, 130.7, 130.3, 130.1, 129.5, 129.2, 123.9, 122.1, 120.0, 118.6, 115.9, 114.0, 111.2, 109.7, 105.8, 105.4, 104.9, 93.7, 77.3, 67.9, 67.5, 66.8, 60.1, 59.5, 46.8, 46.7, 31.9, 30.9, 29.7, 29.6, 29.5, 29.3, 29.1, 29.0, 26.3, 25.5, 24.0, 23.4, 22.7, 14.2, 13.6 ppm; IR (neat): $\tilde{\nu}$= 3114 (w), 2933 (m), 2871 (w), 1727 (s), 1592 (m), 1520 (w), 1455 (s), 1380 (m), 1295 (m), 1246 (s), 1179 (s), 1092 (vs), 1057 (s), 1030 (m), 991 (vs), 950 (w), 840 (m), 829 $cm^{-1}$ (m); UV/Vis ($CHCl_3$): $\lambda_{max}$ ($\varepsilon$)=596 (2300), 559 (11900), 427 (312500), 407 (27700, sh), 307 nm (25500 $M^{-1}cm^{-1}$); HR-MALDI-MS (3-HPA): $m/z$: calcd for $C_{76}H_{80}{}^{15}N_2N_6O_{13}Zn^+$: 1378.5072; found: 1378.5080 $[M]^+$.

**(Tetraethyl 4,4′,4″,4‴-{[10-(2-(1*H*-benzimidazol-7-ylethynyl)-5-{[6-(1*H*-imidazol-1-yl)hexyl]oxy}phenyl)porphyrin-5,15-diyl-κ$N^{21}$,κ$N^{22}$,κ$N^{23}$,κ$N^{24}$]-bis[benzene-2,1,3-triylbis(oxy)]}tetrabutanoato(2−))zinc (3-Zn)**: The title compound was prepared from **18-Zn** (64 mg, 0.05 mmol) according to the general procedure using iodinated precursor **20**. Yield 43 mg (60%); m.p. 109–111 °C; $^1$H NMR ($CDCl_3$, 500 MHz): $\delta$=10.09 (s, 1H; H-C(1)), 9.28 (d, $J$=4.5 Hz, 2H; H-C(3)), 8.94 (d, $J$=4.5 Hz, 2H; H-C(4)), 8.81 (d, $J$= 4.5 Hz, 2H; H-C(8) or H-C(9)), 8.73 (d, $J$=4.5 Hz, 2H; H-C(9) or H-C(8)), 7.82 (d, $J$=8.7 Hz, 1H; H-C(16)), 7.65 (t, $J$=8.3 Hz, 2H; H-C(23)), 7.40 (d, $J$=2.7 Hz, 1H; H-C(13)), 7.27 (dd, $J$=8.7 Hz, 2.7 Hz, 1H; H-C(15)), 6.97 (d, $J$=8.3 Hz, 2H; H-C(22′)), 6.95 (d, $J$=8.3 Hz, 2H; H-C(22)), 6.78 (d, $J$=7.8 Hz, 1H; H-C(42)), 6.73 (d, $J$=7.8 Hz, 1H; H-C(40)), 6.54 (t, $J$=7.8 Hz, 1H; H-C(41)), 4.98 (brs, 1H; H-C(37)), 4.13 (t, $J$=7.7 Hz, 2H; $H_2$-C(30)), 4.01–3.96 (m, 2H; $H_2$-C(24)), 3.94–3.88 (m, 2H; $H_2$-C(24)), 3.84 (q, $J$=7.2 Hz, 4H; $H_2$-C(28′)), 3.70–3.62 (m, 2H; $H_2$-C(24′)), 3.70 (q, $J$=7.2 Hz, 2H; $H_2$-C(28)), 3.59–3.50 (m, 2H; $H_2$-C(24′)), 3.51 (q, $J$=7.2 Hz, 2H; $H_2$-C(28)), 3.27 (brs, 1H; NH), 2.56 (brs, 1H; H-C(45)), 2.54 (brt, $J$=6.0 Hz, 2H; $H_2$-C(35)), 2.20 (brs, 1H; H-C(36)), 2.03 (brs, 1H; H-C(38)), 1.79–1.71 (m, 2H; $H_2$-C(31)), 1.48 (ddd, $J$= 15.3 Hz, 7.6 Hz, 7.6 Hz, 2H; $H_2$-C(26)), 1.31–1.23 (m, 2H; $H_2$-C(25)), 1.18 (ddd, $J$=15.3 Hz, 7.6 Hz, 7.6 Hz, 2H; $H_2$-C(26)), 1.14–1.08 (m, 2H; $H_2$-C(25)), 1.07 (t, $J$=7.0 Hz, 6H; $H_3$-C(29′)), 1.01–0.98 (m, 2H; $H_2$-C(32)), 0.97 (ddd, $J$=14.2 Hz, 7.2 Hz, 7.2 Hz, 2H; $H_2$-C(26′)), 0.91 (t, $J$= 7.0 Hz, 6H; $H_3$-C(29)), 0.86–0.78 (m, 2H; $H_2$-C(25′)), 0.81–0.74 (m, 2H; $H_2$-C(25′)), 0.74–0.70 (m, 2H; $H_2$-C(34)), 0.70 (ddd, $J$=14.2 Hz, 7.2 Hz, 7.2 Hz, 2H; $H_2$-C(26′)), 0.26–0.17 ppm (m, 2H; $H_2$-C(33)); $^{13}$C NMR ($CDCl_3$, 150 MHz): $\delta$=173.22 (C(27′)), 172.56 (C(27)), 159.81 (C(21)), 159.40 (C(21′)), 155.65 (C(14)), 150.74 (C(5)), 150.12 (C(7) or C(10)), 149.92 (C(2)), 148.58 (C(12)), 148.04 (C(10) or C(7)), 140.59 (C(43)), 138.86 (C(45)), 131.94 (C(44)), 131.80 (C(36)), 131.70 (C(3)), 131.29 (C(4)), 131.25 (C(8) or C(9)), 130.80 (C(9) or C(8)), 130.42 (C(16)), 129.62 (C(23)), 123.44 (C(38)), 123.10 (C(40)), 121.56 (C(20)), 120.58 (C(41)), 119.41 (C(17)), 118.69 (C(42)), 117.57 (C(13)), 117.25 (C(11)), 117.16 (C(15)), 115.23 (C(37)), 111.95 (C(6)), 106.18 (C(39)), 105.59 (C(1)), 105.49 (C(22)), 104.87 (C(22′)), 94.66 (C(18)), 88.17 (C(19)), 67.30 (C(24)), 66.65 (C(24′)), 66.39 (C(30)), 59.78 (C(28′) and C(28)), 46.27 (C(35)), 29.69 (C(34)), 29.37 (C(26)), 28.61 (C(26′)), 26.12 (C(31)), 25.66 (C(33)), 24.03 (C(25)), 23.89 (C(32)), 23.11 (C(25′)), 14.10 (C(29′)), 13.87 ppm (C(29)); IR (neat): $\tilde{\nu}$=3362 (w), 2929 (w), 1724 (vs), 1589 (m), 1558 (w), 1520 (w), 1454 (s), 1380 (m), 1357 (w), 1324 (w), 1294 (m), 1281 (m), 1231 (s), 1177 (vs), 1087 (vs), 1056 (vs), 1029 (s), 989 (vs), 940 (m), 838 (m), 829 (m), 793 (s), 716 $cm^{-1}$ (vs); UV/Vis ($CH_2Cl_2$): $\lambda_{max}$ ($\varepsilon$)= 594 (4000), 558 (17000), 426 (447900), 404 (37600, sh), 329 nm (42900 $M^{-1}cm^{-1}$); HR-MALDI-MS (3-HPA): $m/z$: calcd for $C_{80}H_{83}N_8O_{13}Zn^+$: 1427.5366; found: 1427.5390 $[M+H]^+$; elemental analysis calcd (%) for $C_{80}H_{82}N_8O_{13}Zn$ (1428.96): C 67.24, H 5.78, N 7.84; found: C 67.41, H 5.95, N 7.70.

**(Tetraethyl 4,4′,4″,4‴-{[10-(2-(1*H*-indol-7-ylethynyl)-5-{[6-(1*H*-imidazol-1-yl)hexyl]oxy}phenyl)porphyrin-5,15-diyl-κ$N^{21}$,κ$N^{22}$,κ$N^{23}$,κ$N^{24}$]bis[benzene-2,1,3-triylbis(oxy)]}tetrabutanoato(2−))zinc (4-Zn)**: The title compound was prepared from **18-Zn** (50 mg, 0.04 mmol) according to the general procedure using iodinated precursor **21**. Yield 40 mg (74%); m.p. 102–104 °C; $^1$H NMR ($CDCl_3$, 500 MHz): $\delta$=10.06 (s, 1H; H-C(1)), 9.27 (d, $J$=4.3 Hz, 2H; H-C(3)), 8.93 (d, $J$=4.3 Hz, 2H; H-C(4)), 8.78 (d, $J$= 4.5 Hz, 2H; H-C(8) or H-C(9)), 8.73 (d, $J$=4.5 Hz, 2H; H-C(9) or H-C(8)), 7.84 (d, $J$=8.7 Hz, 1H; H-C(16)), 7.64 (t, $J$=8.5 Hz, 2H; H-C(23)), 7.31 (d, $J$=2.6 Hz, 1H; H-C(13)), 7.26 (dd, $J$=8.7 Hz, $J$=2.6 Hz, 1H; H-C(15)), 6.98 (d, $J$=8.6 Hz, 2H; H-C(22′)), 6.92 (d, $J$=8.6 Hz, 2H; H-C(22)), 6.69 (d, $J$=7.6 Hz, 1H; H-C(42)), 6.62 (d, $J$=7.6 Hz, 1H; H-C(40)), 6.40 (t, $J$=7.6 Hz, 1H; H-C(41)), 4.95 (brs, 1H; H-C(37)), 4.54 (dd, $J$=3.0 Hz, 2.0 Hz, 1H; H-C(indole at 3-position)), 4.10 (t, $J$=8.2 Hz, 2H; $H_2$-C(30)), 4.03–3.98 (m, 2H; $H_2$-C(24)), 3.95–3.90 (m, 2H; $H_2$-C(24)), 3.79 (q, $J$=7.2 Hz, 4H; $H_2$-C(28′)), 3.71 (q, $J$=7.2 Hz, 2H; $H_2$-C(28)), 3.61–3.56 (m, 2H; $H_2$-C(24′)), 3.55 (q, $J$=7.2 Hz, 2H; $H_2$-C(28)), 3.54–3.49 (m, 2H; $H_2$-C(24′)), 2.63 (brs, 1H; NH), 2.55 (brt, $J$=6.0 Hz, 2H; $H_2$-C(35)), 2.22 (brs, 1H; H-C(36)), 2.00 (brs, 1H; H-C(38)), 1.75–1.69 (m, 2H; $H_2$-C(31)), 1.62 (s, 1H; H-C(indole at 2-position)), 1.48 (ddd, $J$=16.0 Hz, 8.0 Hz, 8.0 Hz, 2H; $H_2$-C(26)), 1.32–1.24 (m, 2H; $H_2$-C(25)), 1.21 (ddd, $J$=16.0 Hz, 8.0 Hz, 8.0 Hz, 2H; $H_2$-C(26)), 1.16–1.09 (m, 2H; $H_2$-C(25)), 1.02 (t, $J$=7.1 Hz, 6H; $H_3$-C(29′)), 1.01–0.96 (m, 2H; $H_2$-C(32)), 0.93 (t, $J$=7.1 Hz, 6H; $H_3$-C(29)), 0.87–0.79 (m, 2H; $H_2$-C-(26′)), 0.80–0.74 (m, 2H; $H_2$-C(34)), 0.72–0.68 (m, 2H; $H_2$-C(25′)), 0.68–0.64 (m, 2H; $H_2$-C(25′)), 0.63–0.57 (m, 2H; $H_2$-C(26′)), 0.21–0.14 ppm (m, 2H; $H_2$-C(33)); $^{13}$C NMR ($CDCl_3$, 150 MHz): $\delta$=173.28 (C(27′)), 172.61 (C(27)), 159.82 (C(21)), 159.77 (C(21′)), 155.39 (C(14)), 150.62 (C(5)), 150.21 (C(7) or C(10)), 149.66 (C(2)), 148.29 (C(12)), 148.18 (C(10) or C(7)), 134.39 (C(44)), 131.78 (C(36)), 131.38 (C(3)), 131.15 (C(4)), 131.15 (C(8) or C(9)), 130.81 (C(9) or C(8)), 130.53 (C(16)), 129.52 (C(23)), 125.69 (C(43)), 123.47 (C(38)), 122.60 (C(46)), 121.96 (C(20)), 121.86 (C(42)), 119.71 (C(17)), 119.53 (C(40)), 117.95 (C(41)), 117.74 (C(13)), 117.30 (C(11)), 117.17 (C(15)), 115.16 (C(37)), 111.77 (C(6)), 105.82 (C(22)), 105.49 (C(39)), 105.09 (C(1)), 105.00 (C(22′)), 99.34 (C(45)), 94.22 (C(18)), 89.26 (C(19)), 67.36 (C(24)), 66.95 (C(24′)), 66.42 (C(30)), 59.80 (C(28)), 59.63 (C(28′)), 46.23 (C(35)), 31.73 (C(34)), 30.73 (C(26)), 28.60 (C(26′)), 26.20 (C(31)), 24.95 (C(33)), 23.88 (C(25)), 23.83 (C(32)), 23.17 (C(25′)), 14.09 (C(29′)), 14.04 ppm (C(29)); IR (neat): $\tilde{\nu}$=3405 (w), 2931 (m), 2359 (vs), 2340*vs*, 1728 (vs), 1584 (m), 1521 (m), 1455 (vs), 1374 (m), 1295 (m), 1247 (s), 1180 (vs), 1096 (vs), 1058 (m), 1030 (m), 991 (vs), 792 $cm^{-1}$ (s); UV/Vis ($CHCl_3$): $\lambda_{max}$ ($\varepsilon$)= 594 (4000), 558 (19400), 426 (490200), 405 nm (46800 $M^{-1}cm^{-1}$, sh); HR-MALDI-MS (3-HPA): $m/z$: calcd for $C_{81}H_{83}N_7O_{13}Zn^+$: 1425.5335; found: 1425.5380 $[M]^+$; elemental analysis calcd (%) for $C_{81}H_{83}N_7O_{13}Zn$ (1427.98): C 68.13, H 5.86, N 6.87; found: C 68.13, H 5.97, N 6.58.

 © 2009 Wiley-VCH Verlag GmbH & Co. KGaA, Weinheim 

**(Tetraethyl 4,4′,4″,4‴-{[10-(2-(1-methylbenzimidazol-4-ylethynyl)-5-{[6-(1*H*-imidazol-1-yl)hexyl]oxy}phenyl)porphyrin-5,15-diyl-κ$N^{21}$,κ$N^{22}$,κ$N^{23}$,κ$N^{24}$]bis [benzene-2,1,3-triylbis(oxy)]}tetrabutanoato(2−))zinc (5-Zn)**: The title compound was prepared from **18-Zn** (50 mg, 0.04 mmol) according to the general procedure using iodinated precursor **24**. Yield 31 mg (56%); m.p. 103–105 °C; $^1$H NMR ($CD_2Cl_2$, 300 MHz): $\delta$ = 9.99 (s, 1H; H-C(1)), 9.24 (d, $J$ = 4.1 Hz, 2H; H-C(3)), 8.92 (d, $J$ = 4.1 Hz, 2H; H-C(4)), 8.79 (s, 4H; H-C(8) and H-C(9)), 7.97 (d, $J$ = 8.7 Hz, 1H; H-C(16)), 7.71 (t, $J$ = 8.4 Hz, 2H; H-C(23)), 7.46 (brs, 1H; H-C(45)), 7.24 (dd, $J$ = 8.7 Hz, 2.4 Hz, 1H; H-C(15)), 7.05 (d, $J$ = 8.4 Hz, 4H; H-C(22) and H-C(22′)), 6.68 (d, $J$ = 8.1 Hz, 1H; H-C(42)), 6.00 (t, $J$ = 7.8 Hz, 1H; H-C(41)), 5.10 (brs, 1H; H-C(40)), 5.03 (s, 1H; H-C(37)), 4.06–3.85 (m, 6H; $H_2$-C(30), $H_2$-C(24)), 3.86–3.54 (m, 12H; $H_2$-C(28′), $H_2$-C(28), and $H_2$-C(24′)), 3.32 (s, 3H; $H_3$-C(benzimidazole)), 2.56 (brs, 2H; $H_2$-C(35)), 2.38 (brs, 1H; H-C(36)), 2.02 (brs, 1H; H-C(38)), 1.59 (brs, 2H; $H_2$-C(31)), 1.51–1.38 (m, 2H; $H_2$-C(25)), 1.38–1.11 (m, 12H; $H_2$-C(25), $H_2$-C(25′), $H_2$-C(26), and $H_2$-C(26′)), 1.12–1.00 (m, 2H; $H_2$-C(25′)), 0.96 (t, $J$ = 6.9 Hz, 6H; $H_3$-C(29′)), 0.93–0.88 (m, 2H; $H_2$-C(32)), 0.85 (t, $J$ = 6.9 Hz, 6H; $H_3$-C(29)), 0.75 (brs, 2H; $H_2$-C(34)), 0.10 ppm (brs, 2H; $H_2$-C(33)); $^{13}$C NMR ($CDCl_3$, 75 MHz): $\delta$ = 172.8, 172.6, 160.1, 159.8, 150.4, 150.2, 149.3, 149.2, 148.5, 143.1, 134.1, 132.6, 132.0, 131.3, 131.2, 130.9, 130.8, 129.7, 125.4, 123.4, 122.3, 121.8, 119.2, 117.8, 115.9, 114.6, 111.5, 108.7, 106.1, 105.4, 104.8, 94.4, 89.3, 67.8, 67.7, 66.9, 60.2, 60.0, 46.5, 32.3, 31.0, 30.1, 29.8, 29.7, 25.4, 24.4, 24.1, 23.1, 14.2, 14.1 ppm; IR (neat): $\tilde{\nu}$ = 3112 (w), 2924 (m), 2853 (m), 1727 (vs), 1586 (m), 1528 (w), 1496 (w), 1456 (vs), 1415 (w), 1375 (m), 1327 (vs), 1294 (m), 1247 (s), 1182 (vs), 1096 (vs), 1056 (m), 1030 (m), 991 (vs), 779 cm$^{-1}$ (s); UV/Vis ($CHCl_3$): $\lambda_{max}$ ($\varepsilon$) = 598 (6600), 558 (18400), 427 (372200), 406 nm (38000 м$^{-1}$ cm$^{-1}$, sh); HR-MALDI-MS (3-HPA): $m/z$: calcd for $C_{81}H_{84}N_8O_{13}Zn^+$: 1440.5444; found: 1440.5410 $[M+H]^+$.

**General procedure for the metal ion exchange to obtain model complexes 1-Co to 5-Co**: All processes were carried out under $N_2$ atmosphere in the dark. To a solution of the $Zn^{II}$ complex (20 mg, 15.00 μmol) in degassed $CHCl_3$ (4.80 mL), TFA (0.24 mL, 368 mg, 3.2 mmol) was added. The mixture was stirred for 12 min. To the green solution, degassed saturated aqueous solution of $NaHCO_3$ (4.80 mL) was added and the two-phase mixture stirred vigorously until the organic phase turned brown. The colorless aqueous phase was removed by means of a syringe with a long, thin needle. The organic phase was washed with degassed $H_2O$ (2× 4.80 mL) in a similar manner and directly subjected to CC ($Al_2O_3$ neutral; $CH_2Cl_2$ to $CH_2Cl_2$/MeOH 20:1), the product containing fractions were filtered through cotton, and the solvent was removed *in vacuo*. The free-base porphyrin (20 mg, quant.) was obtained as brown amorphous solid. The following steps were carried out in a glove box (oxygen level < 2 ppm, $H_2O$ level < 5 ppm) with carefully degassed and dried solvents. To a degassed solution of the free-base porphyrin (20 mg, 15.00 μmol) in degassed THF (3.30 mL), $CoCl_2$ (18 mg, 140 μmol) and degassed 2,6-lutidine (3 drops) were added and the mixture was stirred in the dark for 12 h. Samples (0.60 mL) of the mixture were directly subjected to CC (degassed $Al_2O_3$ neutral, $CH_2Cl_2$ to $CH_2Cl_2$/MeOH 20:1) to give a mixture of predominantly 1-$Co^{II}$ and some 1-$Co^{III}$, which was analyzed by UV/Vis spectroscopy. After purification, complexes **2-Co**, **3-Co**, and **5-Co** were predominantly found in the $Co^{III}$-oxidation state and had to be reduced. After removing the solvent from the CC purification, the residual solid was dissolved in degassed solvent (1.00 mL) and stirred vigorously with an aqueous solution of $Na_2S_2O_4$ (20 mg in 1.00 mL $H_2O$) for 30 min. The organic phase was analyzed by UV/Vis spectroscopy and revealed predominant reduction of $Co^{III}$ to $Co^{II}$. The solvent was again removed *in vacuo*, and fresh solvent (0.10 mL) was added. The resulting solution was directly used for the EPR studies. Complex **4-Co** was predominantly found in the $Co^{II}$ oxidation state after CC. Complex **1-Co** was measured in $CH_2Cl_2$, $CD_2Cl_2$, and toluene as solvent, complex **3-Co** in $CHCl_3$ as solvent, complexes **2-Co, $^{15}$N-2-Co**, **4-Co**, and **5-Co** were measured in $CH_2Cl_2$ as solvent, complexes **6-Co**-DiMeIm and **7-Co**-DiMeIm were measured in toluene as solvent.

**(Tetraethyl 4,4′,4″,4‴-{[10-(2-(1*H*-imidazol-5-ylethynyl)-5-{[6-(1*H*-imidazol-1-yl)hexyl]oxy}phenyl)porphyrin-5,15-diyl-κ$N^{21}$,κ$N^{22}$,κ$N^{23}$,κ$N^{24}$]bis-[benzene-2,1,3-triylbis(oxy)]}tetrabutanoato(2−))cobalt (2-Co)**: M.p. 137 °C (decomp); IR (neat): $\tilde{\nu}$ = 2922 (s), 2853 (m), 1727 (s), 1660 (m), 1594 (m), 1457 (s), 1375 (m), 1338 (m), 1291 (m), 1247 (s), 1178 (s), 1096 (vs), 1066 (s), 1026 (s), 1002 (vs), 843 (m), 794 cm$^{-1}$ (s); UV/Vis ($CHCl_3$): **2-$Co^{II}$**, $\lambda_{max}$ = 408, 529 nm; **2-$Co^{III}$**, $\lambda_{max}$ = 429, 539 nm; HR-MALDI-MS (HPA): $m/z$: calcd for $C_{76}H_{80}CoN_8O_{13}^+$: 1371.5177; found: 1371.5200 $[M]^+$.

**(Tetraethyl 4,4′,4″,4‴-{[10-(2-(1*H*-imidazol-5-ylethynyl)-5-{[6-(1*H*-[1,3-15$N^2$]imidazol-1-yl)hexyl]oxy}phenyl)porphyrin-5,15-diyl-κ$N^{21}$,κ$N^{22}$,κ$N^{23}$,κ$N^{24}$]bis[benzene-2,1,3-triylbis(oxy)]}tetrabutanoato(2−))cobalt ($^{15}$N-2-Co)**: M.p. 130 °C (decomp); IR (neat): $\tilde{\nu}$ = 2953 (m), 2925 (m), 2858 (m), 1724 (vs), 1595 (m), 1456 (s), 1376 (m), 1288 (s), 1270 (s), 1249 (vs), 1228 (s), 1178 (s), 1093 (vs), 1070 (vs), 1023 (s), 1002 (vs), 843 (m), 794 cm$^{-1}$ (s); UV/Vis ($CHCl_3$): **$^{15}$N-2-$Co^{II}$**, $\lambda_{max}$ = 408, 529 nm; **$^{15}$N-2-$Co^{III}$**, $\lambda_{max}$ = 429, 539 nm; HR-MALDI-MS (HPA): $m/z$: calcd for $C_{76}H_{80}CoN_6{}^{15}N_2O_{13}{}^+$: 1373.5118; found: 1373.5140 $[M]^+$.

**(Tetraethyl 4,4′,4″,4‴-{[10-(2-(1*H*-benzimidazol-7-ylethynyl)-5-{[6-(1*H*-imidazol-1-yl)hexyl]oxy}phenyl)porphyrin-5,15-diyl-κ$N^{21}$,κ$N^{22}$,κ$N^{23}$,κ$N^{24}$]bis-[benzene-2,1,3-triylbis(oxy)]}tetrabutanoato(2−))cobalt (3-Co)**: M.p. 145 °C (decomp); IR (neat): $\tilde{\nu}$ = 2925 (m), 2867 (w), 1726 (vs), 1592 (m), 1455 (s), 1417 (w), 1373 (m), 1290 (m), 1247 (s), 1231 (s), 1178 (vs), 1094 (vs), 1063 (s), 1025 (s), 1003 (s), 842 (w), 794 cm$^{-1}$ (s); UV/Vis ($CHCl_3$): **3-$Co^{II}$**, $\lambda_{max}$ = 408, 529 nm; **3-$Co^{III}$**, $\lambda_{max}$ = 429, 540 nm; HR-MALDI-MS (HPA): $m/z$: calcd for $C_{80}H_{82}CoN_8O_{13}^+$: 1421.5333; found: 1421.5310 $[M]^+$.

**(Tetraethyl 4,4′,4″,4‴-{[10-(2-(1*H*-indol-7-ylethynyl)-5-{[6-(1*H*-imidazol-1-yl)hexyl]oxy}phenyl)porphyrin-5,15-diyl-κ$N^{21}$,κ$N^{22}$,κ$N^{23}$,κ$N^{24}$]-bis-[benzene-2,1,3-triylbis(oxy)]}tetrabutanoato(2−))cobalt (4-Co)**: M.p. 98 °C (decomp); IR (neat): $\tilde{\nu}$ = 3401 (w), 2923 (m), 2853 (w), 1726 (s), 1592 (m), 1584 (m), 1456 (s), 1374 (m), 1331 (m), 1313 (m),1290 (m), 1248 (s), 1178 (vs), 1093 (vs), 1062 (s), 1026 (s), 995 (vs), 887 (w), 843 (m), 793 cm$^{-1}$ (s); UV/Vis ($CHCl_3$): **4-$Co^{II}$**, $\lambda_{max}$ = 408, 529 nm; **4-$Co^{III}$**, $\lambda_{max}$ = 429, 540 nm; HR-MALDI-MS (HPA): $m/z$: calcd for $C_{81}H_{83}CoN_7O_{13}^+$: 1420.5381; found: 1420.5360 $[M]^+$.

**(Tetraethyl 4,4′,4″,4‴-{[10-(2-(1-methylbenzimidazol-4-ylethynyl)-5-{[6-(1*H*-imidazol-1-yl)hexyl]oxy}phenyl)porphyrin-5,15-diyl-κ$N^{21}$,κ$N^{22}$,κ$N^{23}$,κ$N^{24}$]bis-[benzene-2,1,3-triylbis(oxy)]}tetrabutanoato(2−))cobalt (5-Co)**: M.p. 96 °C (decomp); IR (neat): $\tilde{\nu}$ = 2930 (w), 2868 (w), 1723 (vs), 1585 (m), 1494 (w), 1456 (s), 1414 (m), 1374 (m), 1287 (m), 1248 (s), 1230 (s), 1178 (vs), 1090 (vs), *1062* (vs), 1026 (s), 995 (s), 842 (w), 793 cm$^{-1}$ (s); UV/Vis ($CHCl_3$): **5-$Co^{II}$**, $\lambda_{max}$ = 409, 529 nm; **5-$Co^{III}$**, $\lambda_{max}$ = 427, 537 nm; HR-MALDI-MS (HPA): $m/z$: calcd for $C_{81}H_{84}CoN_8O_{13}^+$: 1435.5484; found: 1435.5470 $[M]^+$.

**Deuterium exchange of the cobalt complexes**: Deuterium exchange was achieved by vigorously stirring solutions of **1-Co** and **3-Co** (4 mg each) in $CH_2Cl_2$ (1.00 mL) with $Na_2S_2O_4$ (20 mg) in $D_2O$ (1.00 mL) for 30 min and stirring a solution of **7-Co**-DiMeIm (4 mg) in toluene (1 mL) with $Na_2S_2O_4$ (20 mg) in $D_2O$ (1.00 mL) for 4 h. The organic phase was directly used for the measurements.

## Acknowledgements

This work was supported by the Swiss National Science Foundation, the NCCR "Nanoscale Science" Basel, and ETH Zurich. We are grateful to Joerg Forrer for technical support.

[1] E. L. Raven, A. G. Mauk, *Adv. Inorg. Chem.* **2000**, *51*, 1–50.
[2] J. R. Tame, B. Vallone, *Acta Crystallogr. Sect. D* **2000**, *56*, 805–811.
[3] N. C. Veitch, A. T. Smith, *Adv. Inorg. Chem.* **2000**, *51*, 107–162.
[4] H. Dube, B. Kasumaj, C. Calle, M. Saito, G. Jeschke, F. Diederich, *Angew. Chem.* **2008**, *120*, 2638–2642; *Angew. Chem. Int. Ed.* **2008**, *47*, 2600–2603.
[5] a) B. Felber, C. Calle, P. Seiler, A. Schweiger, F. Diederich, *Org. Biomol. Chem.* **2003**, *1*, 1090–1093; b) B. Felber, F. Diederich, *Helv. Chim. Acta* **2005**, *88*, 120–153; c) B. Felber, PhD thesis Nr. 15058, ETH Zurich, **2003**.

 © 2009 Wiley-VCH Verlag GmbH & Co. KGaA, Weinheim 

[6] J. J. P. Steward, Fujitsu Limited **2001**, MOPAC **2002**.
[7] S. E. V. Phillips, B. P. Schoenborn, *Nature* **1981**, *292*, 81–82.
[8] B. J. Littler, M. A. Miller, C.-H. Hung, R. W. Wagner, D. F. O'Shea, P. D. Boyle, J. S. Lindsey, *J. Org. Chem.* **1999**, *64*, 1391–1396.
[9] P. J. Dandliker, F. Diederich, A. Zingg, J.-P. Gisselbrecht, M. Gross, A. Louati, E. Sanford, *Helv. Chim. Acta* **1997**, *80*, 1773–1801.
[10] A. M. Matos Beja, J. A. Paixao, M. R. Ramos Silva, L. Alte da Veiga, A. M. d. À. Rocha Gonsalves, A. C. Serra, *Acta Crystallogr. Sect. C* **2000**, *56*, 354–355.
[11] P. Weyermann, F. Diederich, *Helv. Chim. Acta* **2002**, *85*, 599–617.
[12] F. B. Panosyan, W. J. Still, *Can. J. Chem.* **2001**, *79*, 1110–1114.
[13] D. J. Rabiger, M. M. Joullie, *J. Org. Chem.* **1961**, *26*, 1649–1650.
[14] Y. Kondo, S. Kojima, T. Sakamoto, *Heterocycles* **1996**, *43*, 2741–2746.
[15] A. Marcos, C. Pedregal, C. Avendano, *Tetrahedron* **1991**, *47*, 7459–7464.
[16] a) C.-Z. Li, K. Nishiyama, I. Taniguchi, *Electrochim. Acta* **2000**, *45*, 2883–2888; b) M. C. Marden, L. Kiger, C. Poyart, A. K. Rashid, J. Kister, F. Stetzkowski-Marden, G. Caron, M. Haque L. Moens, *FEBS Lett.* **2000**, *472*, 221–224.
[17] a) H. Adams, K. D. M. Harris, G. A. Hembury, C. A. Hunter, D. Livingstone, J. F. McCabe, *Chem. Commun.* **1996**, 2531–2532; b) C. Allott, H. Adams, P. L. Bernad, Jr., C. A. Hunter, C. Rotger, J. A. Thomas, *Chem. Commun.* **1998**, 2449–2450; c) E. A. Meyer, R. K. Castellano, F. Diederich, *Angew. Chem.* **2003**, *115*, 1244–1287; *Angew. Chem. Int. Ed.* **2003**, *42*, 1210–1250.
[18] S. Stoll, C. Calle, G. Mitrikas, A. Schweiger, *J. Magn. Reson.* **2005**, *177*, 93–101.
[19] a) Pulsed Davies-ENDOR is described in: C. Fan, P. E. Doan, C. E. Davoust, B. M. Hoffman, *J. Magn. Reson.* **1992**, *98*, 62–72; b) E. R. Davies, *Phys. Lett. A* **1974**, *47*, 1–2.
[20] K. Shikama, *Prog. Biophys. Mol. Biol.* **2006**, *91*, 83–162.
[21] B. Kasumaj, S. Stoll, *J. Magn. Reson.* **2008**, *190*, 233–247.
[22] a) See: S. Van Doorslaer, A. Schweiger, B. Kraeutler, *J. Phys. Chem. B* **2001**, *105*, 7554–7563; and references therein; b) for the stereoelectronic structure of Co-Mb-$O_2$ see: L. C. Dickinson, J. C. W. Chien, *Proc. Natl. Acad. Sci. USA* **1980**, *77*, 1235–1239.
[23] A. Schweiger, G. Jeschke, *Principles of Pulse Electron Paramagnetic Resonance*, Oxford University Press, Oxford, **2001**.
[24] I. Gromov, J. Shane, J. Forrer, R. Rakhmatoullin, Y. Rozentzwaig, A. Schweiger, *J. Magn. Reson.* **2001**, *149*, 196–203.
[25] S. Stoll, A. Schweiger, *J. Magn. Reson.* **2006**, *178*, 42–55.

Received: October 8, 2008
Published online: December 3, 2008

 © 2009 Wiley-VCH Verlag GmbH & Co. KGaA, Weinheim 